Journal of Computational Physics 229 (2010) 5228–5245

Contents lists available at ScienceDirect

Journal of Computational Physics

journal homepage: www.elsevier.com/locate/jcp

Adjoint wall functions: A new concept for use in aerodynamic shape optimization

A.S. Zymaris [a], D.I. Papadimitriou [a], K.C. Giannakoglou [a,*], C. Othmer [b]

[a] National Technical University of Athens, School of Mechanical Engineering, Parallel CFD & Optimization Unit, P.O. Box 64069, 15710 Athens, Greece
[b] Volkswagen AG, CAE Methods, Group Research, Letter Box 1777, D-38436 Wolfsburg, Germany

ARTICLE INFO

Article history:
Received 30 September 2009
Received in revised form 22 February 2010
Accepted 24 March 2010
Available online 27 March 2010

Keywords:
Continuous adjoint method
Sensitivity derivatives
Optimization
Navier–Stokes equations
Turbulence
Wall functions

ABSTRACT

The continuous adjoint method for the computation of sensitivity derivatives in aerodynamic optimization problems of steady incompressible flows, modeled through the k–ε turbulence model with wall functions, is presented. The proposed formulation leads to the adjoint equations along with their boundary conditions by introducing the *adjoint to the friction velocity*. Based on the latter, an *adjoint law of the wall* that bridges the gap between the solid wall and the first grid node off the wall is proposed and used during the solution of the system of adjoint (to both the mean flow and turbulence) equations. Any high Reynolds turbulence model, other than the k–ε one used in this paper, could also profit from the proposed adjoint wall function technique. In the examined duct flow problems, where the total pressure loss due to viscous effects is used as objective function, emphasis is laid on the accuracy of the computed sensitivity derivatives, rather than the optimization itself. The latter might rely on any descent method, once the objective function gradient has accurately been computed.

1. Introduction

In aerodynamic shape optimization problems, the adjoint method computes (or, depending on the simplifications made, approximates) the gradient of the objective function with respect to the design variables, by solving the system of adjoint equations which are deduced from the mathematical theory for the control of systems governed by pde's. Governing pde's are the flow model equations, coupled with appropriate boundary conditions. The cost of solving the system of adjoint equations is comparable to the cost of solving the flow equations, irrespective of the number of design variables, in contrast to finite differences or the complex variable approach, [1,2]. A repetitive process, with cycles comprising the numerical solution of the state and adjoint systems of equations, the gradient computation and a gradient-based descent step, is usually carried out until the design converges to the optimal solution, not necessarily the global one. Alternatively, efficient one-shot approaches, [3], in which the state, adjoint and correction equations are coupled, can be used. In this paper, we restrict ourselves to the exact computation of the objective function gradient in problems governed by flow equations based on the wall function technique and refrain from comparing gradient-based optimization variants.

It is known that the discrete form of the adjoint equations can be obtained according to either the continuous or the discrete adjoint approach. In the former, [4–7], the adjoint pde's and their boundary conditions are derived by developing the variation in the objective function augmented by the state (flow) equations after multiplying them by the adjoint variables.

* Corresponding author. Tel.: +30 210 772 1636; fax: +30 210 772 1658.
E-mail addresses: azymar@mail.ntua.gr (A.S. Zymaris), dpapadim@mail.ntua.gr (D.I. Papadimitriou), kgianna@central.ntua.gr (K.C. Giannakoglou), carsten.othmer@volkswagen.de (C. Othmer).

0021-9991/$ - see front matter © 2010 Elsevier Inc. All rights reserved.
doi:10.1016/j.jcp.2010.03.037

The adjoint equations are, subsequently, discretized using schemes similar to those used for the state equations. On the other hand, in the discrete adjoint method, [8–11], the state equations are discretized first and the discrete adjoint equations are deduced from the discrete state equations. This paper is concerned only with the continuous adjoint method. We shall, therefore, refrain from commenting upon the discrete adjoint method, unless this is absolutely necessary. Also, any comparison between continuous and discrete adjoints is beyond the scope of this paper.

Given an objective function that reflects the designer's requirements, the continuous adjoint approach starts by selecting the flow model, namely the system of state pde's. Dealing with turbulent flows, the state pde's comprise the mean-flow and turbulence model equations. An exact adjoint formulation must take into consideration variations in both of them. However, in the majority of relevant papers based on the adjoint method, the common practice is to neglect variations in the turbulence variables, [6,7,12,13]. This is usually referred to as the "*frozen turbulence assumption*"; neglecting variations in turbulence variables makes the whole mathematical development less burdensome and reduces the number of adjoint equations to be solved. The price to pay is the reduced accuracy in the computed gradient. Recently, the present authors proposed, [14], the exact adjoint to the Spalart–Allmaras one-equation turbulence model [15] and quantified the loss in the gradient accuracy caused by omitting this extra adjoint equation. The extension of the (exact) continuous adjoint approach to the two-equation k–ε turbulence model was a prerequisite for the development of the proposed adjoint wall function technique. Note that, to the authors knowledge, apart from [14], only a few papers account for variations in turbulence model variables and all of them are based on the discrete adjoint approach, [16–22].

The present paper proposes a new continuous adjoint formulation for steady flow problems in which the state equations include a high Reynolds number turbulence model based on the wall function technique, [23–26]. With the latter, the entire turbulent boundary layer does not need to be solved and the law of the wall bridges the gap between the solid walls on which the boundary layer is developed and the adjacent grid nodes generated with a large grid spacing. So, the state equations are solved on grids which are much coarser than those required by the low Reynolds number models, leading to less demanding computations. High Reynolds number turbulence models are often used for industrial computations, as "everyday" flow analysis tools. The shear stress (or, equivalently, the friction velocity), deduced from the wall functions, substitutes the diffusion fluxes in the discretized momentum (and energy, in compressible flows) equations at nodes adjacent to the wall, where the standard finite difference schemes cannot be applied. The adjoint to the high Reynolds turbulence model presented in this paper introduces what should be referred to as the *adjoint wall function* technique, by defining and using the so-called *adjoint friction velocity*. Though this paper is restricted to a specific high-Reynolds turbulence model (k–ε), any other eddy-viscosity turbulence model based on the wall function technique (such as the high-Reynolds number variant of the Spalart–Allmaras model, [15]) could be used in place of the k–ε model. Through a similar development, the adjoint equations, their boundary conditions as well as new terms in the sensitivity derivatives can be derived. The adjoint wall function technique could even be applied to flow solvers coupled with Large Eddy Simulation (LES) models (namely, their wall functions based variants, [27–30]), provided that the adjoint to the LES pde's are available.

Without loss of generality, the present applications are restricted to duct flows. The objective function is an integral quantity along the inlet to and the outlet from the flow domain, expressing the total pressure losses due to viscous flow effects. Note that [14] dealt with the same objective function, using however the low-Reynolds Spalart–Allmaras model. Similarly to [14], the present paper handles the objective function (symbol J, see below) as a separate term in the development of the adjoint equations. So, the reader may readily replace J with any other objective function (see, for instance, similar works by the same authors, [7,31]). In the absence of field integrals in J, this will lead to the same adjoint equations, different adjoint boundary conditions and different sensitivity derivatives.

Finally, let us make clear that this paper deals with steady flows only. Any extension to unsteady flows is expected to have much higher memory requirements and CPU cost. However, accommodating the new adjoint wall function technique in such an unsteady method is expected to be straightforward. Adjoint methods for unsteady flows are beyond the scope of this paper and the interested reader should refer to [32,33] or [34]; the latter is a "rival" derivative-free approach for designs based on unsteady flow considerations.

2. Development of the continuous adjoint approach

2.1. Objective function and flow equations

The objective function J to be minimized stands for the total pressure losses between the inlet (S_i) to and the outlet (S_o) from the flow domain. Thus,

$$J = -\int_{S_i}\left(p+\frac{1}{2}v_i^2\right)v_k n_k\,dS - \int_{S_o}\left(p+\frac{1}{2}v_i^2\right)v_k n_k\,dS \tag{1}$$

where p is the static pressure divided by the constant density, v_i the velocity components and n_k components of the normal to the boundary outward unit vector. As already mentioned in Section 1, during the development of the adjoint equations, J will be kept apart from the remaining terms, as much as possible. So, those who wish to replace Eq. (1) with any other objective function may certainly benefit from what follows. It should be stressed that the objective function J, Eq. (1), includes integrals defined along boundaries (inlet, outlet) other than solid walls with respect to the shape variables of which the

sensitivity derivatives are to be computed. This increases the complexity of the adjoint boundary conditions. For further discussion, the interested reader should refer to [31].

The flow model consists of the Navier–Stokes equations for incompressible fluids and the standard k–ε turbulence model with wall functions [35]. The mean flow equations are given by

$$\begin{aligned} R_i^v &= v_j \frac{\partial v_i}{\partial x_j} + \frac{\partial p_{eff}}{\partial x_i} - \frac{\partial}{\partial x_j}\left[(\nu + \nu_t)\left(\frac{\partial v_i}{\partial x_j} + \frac{\partial v_j}{\partial x_i}\right)\right] = 0 \quad (i = 1,2,3) \\ R^p &= \frac{\partial v_j}{\partial x_j} = 0 \end{aligned} \tag{2}$$

where ν and ν_t are the laminar and turbulent viscosity coefficients and x_i are the Cartesian coordinates. According to the Einstein convention, repeated indices imply summation.

The high Reynolds k–ε model equations read

$$\begin{aligned} R^k &= v_j \frac{\partial k}{\partial x_j} - \frac{\partial}{\partial x_j}\left[\left(\nu + \frac{\nu_t}{Pr_k}\right)\frac{\partial k}{\partial x_j}\right] - P_k + \varepsilon = 0 \\ R^\varepsilon &= v_j \frac{\partial \varepsilon}{\partial x_j} - \frac{\partial}{\partial x_j}\left[\left(\nu + \frac{\nu_t}{Pr_\varepsilon}\right)\frac{\partial \varepsilon}{\partial x_j}\right] - c_1 P_k \frac{\varepsilon}{k} + c_2 \frac{\varepsilon^2}{k} = 0 \end{aligned} \tag{3}$$

where k is the turbulent kinetic energy, ε is the turbulent energy dissipation and

$$P_k = \tau_{ij}\frac{\partial v_i}{\partial x_j} = \nu_t\left(\frac{\partial v_i}{\partial x_j} + \frac{\partial v_j}{\partial x_i}\right)\frac{\partial v_i}{\partial x_j} \tag{4}$$

is the production of k. The turbulent viscosity coefficient ν_t is given by

$$\nu_t = c_\mu \frac{k^2}{\varepsilon} \tag{5}$$

The model constants are $c_\mu = 0.09$, $c_1 = 1.44$, $c_2 = 1.92$, $Pr_k = 1.0$, $Pr_\varepsilon = 1.3$ [35]. In Eq. (2), p_{eff} stands for $p + \frac{2}{3}k$.

In internal aerodynamics, Dirichlet conditions are imposed on v_i, k and ε and zero Neumann condition for p at the inlet. At the outlet, zero Neumann conditions are imposed on v_i, k and ε whereas the exit pressure is fixed.

In this paper, Eqs. (2) and (3) are solved on unstructured grids with triangular elements using a vertex-centered, finite volume scheme. The pseudo-compressibility approach is used, [36]. This is based on the Roe's approximate Riemann solver, [37], MUSCL interpolation for computing second-order accurate convection terms and the P_1 element assumption (constant gradient of the flow variables within each grid element) for the diffusion terms.

The integration of the governing equations over the finite volumes leads to the balance of inviscid and viscous fluxes crossing their boundaries along with volume integrals of source terms, if any. Apart from the boundary nodes where Dirichlet conditions are imposed, any other boundary condition is satisfied in the weak sense, by modifying the fluxes crossing the corresponding finite volume boundary segments ($\alpha\beta$; Fig. 1)

In this paper, the wall function technique with slip velocities is applied [23–26]. According to this model, the "real" solid wall is assumed to lie at distance Δ underneath the grid boundary marked as "solid wall"; the governing equations are discretized over the finite volume of the "solid wall" node P (Fig. 1) by taking into consideration (in the weak sense) that the velocity at P is tangent to the wall and conforms to the so-called wall functions that bridge the gap between P and the "real" wall. Along the ("solid wall") boundary segment $\alpha\beta$, the convective flux is zero (no-penetration condition) whereas the diffusion one depends on the friction velocity v_τ, defined by

$$v_\tau^2 = (\nu + \nu_t)\left(\frac{\partial v_i}{\partial x_j} + \frac{\partial v_j}{\partial x_i}\right) n_j t_i \tag{6}$$

and computed via the law of the wall. In the sake of convenience, v_τ^2 instead of the signed (but not differentiable at $v_\tau = 0$) quantity $v_\tau\,|v_\tau|$ will be used.

In the log law region and the viscous sublayer, the tangential to the wall velocity profile ($v_i t_i$, where t_i are the tangent unit vector components; abbreviated to v_t) in wall coordinates $\left(y^+ = \frac{\Delta v_\tau}{\nu},\ v^+ = \frac{v_t}{v_\tau}\right)$ results from

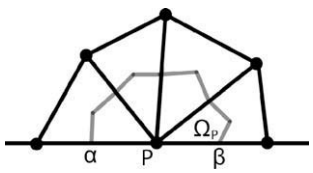

Fig. 1. A 2D example: a vertex-centered finite volume Ω_P associated with the boundary node P. Segment $\alpha\beta$ of the finite volume boundary may belong to either the inlet/outlet boundaries or the "solid wall" boundary, depending on the context of the section referring to this figure.

$$\begin{aligned} v^+ &= \tfrac{1}{\kappa}\ln y^+ + B, \quad y^+ \geqslant y_c^+ \\ v^+ &= y^+, \qquad\qquad y^+ < y_c^+ \end{aligned} \tag{7}$$

where y_c^+ is deduced from solving $y_c^+ = \frac{1}{\kappa}\ln y_c^+ + B$, $\kappa = 0.41$ and $B = 5.5$. Boundary conditions for k and ε at P (Fig. 1) are defined depending on whether P lies within the log law region or the viscous sublayer. These are as follows [23–26]:

$$k_P = \frac{v_\tau^2}{\sqrt{c_\mu}}, \quad \varepsilon_P = \frac{v_\tau^3}{\kappa \Delta}, \quad y^+ \geqslant y_c^+ \quad k_P = \frac{v_\tau^2}{\sqrt{c_\mu}}\left(\frac{y^+}{y_c^+}\right)^2, \quad \varepsilon_P = k_P^{\frac{3}{2}} \frac{1 + \frac{5.3\nu}{\sqrt{k_P}\Delta}}{\kappa c_\mu^{-\frac{3}{4}} \Delta}, \quad y^+ < y_c^+ \tag{8}$$

2.2. Augmented objective function

By introducing the adjoint variables u_i, q, k_a and ε_a, corresponding to the primal (or state) variables v_i, p, k and ε, respectively, the augmented objective function is

$$L = J + \int_\Omega \left(u_i R_i^v + q R^p + k_a R^k + \varepsilon_a R^\varepsilon\right) d\Omega \tag{9}$$

where J is given by Eq. (1) and Ω denotes the flow domain. Using the Leibniz integral rule the sensitivities of the L with respect to the design variables b_m read

$$\frac{\delta L}{\delta b_m} = \frac{\delta J}{\delta b_m} + \int_\Omega \left(u_i \frac{\delta R_i^v}{\delta b_m} + q\frac{\delta R^p}{\delta b_m} + k_a \frac{\delta R^k}{\delta b_m} + \varepsilon_a \frac{\delta R^\varepsilon}{\delta b_m}\right) d\Omega + \int_\Omega \left(u_i R_i^v + q R^p + k_a R^k + \varepsilon_a R^\varepsilon\right) \frac{\delta(d\Omega)}{\delta b_m} \tag{10}$$

Since, in Eq. (10), the last two integrals are all equal to zero, computing $\frac{\delta J}{\delta b_m}$ is equivalent to computing $\frac{\delta L}{\delta b_m}$. The adjoint variables u_i, q, k_a and ε_a act as Lagrange multipliers which are to be computed at all grid nodes by solving the adjoint pde's. The latter can be derived after identifying and eliminating all field integrals in Eq. (10) that depend on $\frac{\partial v_i}{\partial b_m}$, $\frac{\partial p}{\partial b_m}$, $\frac{\partial k}{\partial b_m}$ and $\frac{\partial \varepsilon}{\partial b_m}$. The elimination of the corresponding boundary integrals gives rise to the adjoint boundary conditions. The remaining terms in Eq. (10) depend on the previously computed u_i, q, k_a and ε_a fields and stand for the derivatives of J with respect to b_m (sensitivity derivatives), [7,31]. By taking into account that [7]

$$\frac{\delta(d\Omega)}{\delta b_m} = \frac{\partial}{\partial x_k}\left(\frac{\delta x_k}{\delta b_m}\right) d\Omega \tag{11}$$

and by expressing the total sensitivities $\frac{\delta()}{\delta b_m}$ in terms of the partial ones $\frac{\partial()}{\partial b_m}$ and the sensitivities $\frac{\delta x_k}{\delta b_m}$ of grid nodes, namely

$$\frac{\delta()}{\delta b_m} = \frac{\partial()}{\partial b_m} + \frac{\partial()}{\partial x_k}\frac{\delta x_k}{\delta b_m} \tag{12}$$

the application of the Green–Gauss theorem leads to

$$\frac{\delta L}{\delta b_m} = \frac{\delta J}{\delta b_m} + \int_\Omega \left(u_i \frac{\partial R_i^v}{\partial b_m} + q\frac{\partial R^p}{\partial b_m} + k_a \frac{\partial R^k}{\partial b_m} + \varepsilon_a \frac{\partial R^\varepsilon}{\partial b_m}\right) d\Omega + \int_S \left(u_i R_i^v + q R^p + k_a R^k + \varepsilon_a R^\varepsilon\right) \frac{\delta x_k}{\delta b_m} n_k \, dS \tag{13}$$

where S is the boundary of Ω. By considering the imposed boundary conditions and the invariance of the inlet/outlet grid nodal coordinates with respect to the design variables $\left(\frac{\delta x_k}{\delta b_m}\Big|_{S_i,S_o} = 0\right)$, the sensitivities of the objective function become

$$\frac{\delta J}{\delta b_m} = -\int_{S_i} \frac{\partial p}{\partial b_m} v_k n_k \, dS - \int_{S_o} \left(v_i \frac{\partial v_i}{\partial b_m} v_k n_k + \frac{1}{2} v_i^2 \frac{\partial v_k}{\partial b_m} n_k\right) dS \tag{14}$$

The partial sensitivities of the mean flow and turbulent model equations, which appear in the field integral of Eq. (13), are given by

$$\frac{\partial R_i^v}{\partial b_m} = \frac{\partial v_j}{\partial b_m}\frac{\partial v_i}{\partial x_j} + v_j \frac{\partial}{\partial x_j}\left(\frac{\partial v_i}{\partial b_m}\right) + \frac{\partial}{\partial x_i}\left(\frac{\partial p_{eff}}{\partial b_m}\right) - \frac{\partial}{\partial x_j}\left[\frac{\partial v_t}{\partial b_m}\left(\frac{\partial v_i}{\partial x_j} + \frac{\partial v_j}{\partial x_i}\right)\right] - \frac{\partial}{\partial x_j}\left\{(\nu + \nu_t)\left[\frac{\partial}{\partial x_j}\left(\frac{\partial v_i}{\partial b_m}\right) + \frac{\partial}{\partial x_i}\left(\frac{\partial v_j}{\partial b_m}\right)\right]\right\} \tag{15a}$$

$$\frac{\partial R^p}{\partial b_m} = \frac{\partial}{\partial x_j}\left(\frac{\partial v_j}{\partial b_m}\right) \tag{15b}$$

$$\frac{\partial R^k}{\partial b_m} = \frac{\partial v_j}{\partial b_m}\frac{\partial k}{\partial x_j} + v_j \frac{\partial}{\partial x_j}\left(\frac{\partial k}{\partial b_m}\right) - \frac{\partial}{\partial x_j}\left[\left(\nu + \frac{\nu_t}{Pr_k}\right)\frac{\partial}{\partial x_j}\left(\frac{\partial k}{\partial b_m}\right)\right] - \frac{1}{Pr_k}\frac{\partial}{\partial x_j}\left(\frac{\partial v_t}{\partial b_m}\frac{\partial k}{\partial x_j}\right) - \frac{\partial P_k}{\partial b_m} + \frac{\partial \varepsilon}{\partial b_m} \tag{15c}$$

$$\begin{aligned} \frac{\partial R^\varepsilon}{\partial b_m} = {} & \frac{\partial v_j}{\partial b_m}\frac{\partial \varepsilon}{\partial x_j} + v_j \frac{\partial}{\partial x_j}\left(\frac{\partial \varepsilon}{\partial b_m}\right) - \frac{\partial}{\partial x_j}\left[\left(\nu + \frac{\nu_t}{Pr_\varepsilon}\right)\frac{\partial}{\partial x_j}\left(\frac{\partial \varepsilon}{\partial b_m}\right)\right] - \frac{1}{Pr_\varepsilon}\frac{\partial}{\partial x_j}\left(\frac{\partial v_t}{\partial b_m}\frac{\partial \varepsilon}{\partial x_j}\right) \\ & - c_1 \frac{\partial P_k}{\partial b_m}\frac{\varepsilon}{k} - c_1 P_k \frac{1}{k}\frac{\partial \varepsilon}{\partial b_m} + c_1 P_k \frac{\varepsilon}{k^2}\frac{\partial k}{\partial b_m} + 2c_2 \frac{\varepsilon}{k}\frac{\partial \varepsilon}{\partial b_m} - c_2 \frac{\varepsilon^2}{k^2}\frac{\partial k}{\partial b_m} \end{aligned} \tag{15d}$$

The sensitivities of ν_t are deduced from Eq. (5),

$$\frac{\partial \nu_t}{\partial b_m} = 2c_\mu \frac{k}{\varepsilon}\frac{\partial k}{\partial b_m} - c_\mu \frac{k^2}{\varepsilon^2}\frac{\partial \varepsilon}{\partial b_m} \tag{16}$$

2.3. Adjoint formulation

It is a matter of mathematical rearrangements, based on the application of the Green–Gauss theorem and the use of Eqs. (15a) and (16), to express Eq. (13) as follows:

$$\begin{aligned}\frac{\delta L}{\delta b_m} = \frac{\delta J}{\delta b_m} &+ \int_\Omega \left(R_i^u \frac{\partial \nu_i}{\partial b_m} + R^q \frac{\partial p}{\partial b_m} + R^{k_a}\frac{\partial k}{\partial b_m} + R^{\varepsilon_a}\frac{\partial \varepsilon}{\partial b_m}\right) d\Omega + \int_S \left(D_i^u \frac{\partial \nu_i}{\partial b_m} + D^q \frac{\partial p}{\partial b_m} + D^{k_a}\frac{\partial k}{\partial b_m} + D^{\varepsilon_a}\frac{\partial \varepsilon}{\partial b_m}\right) dS \\ &- \int_S (\nu+\nu_t) u_i \frac{\partial}{\partial b_m}\left(\frac{\partial \nu_i}{\partial x_j} + \frac{\partial \nu_j}{\partial x_i}\right) n_j\, dS - \int_S k_a \left(\nu + \frac{\nu_t}{Pr_k}\right)\frac{\partial}{\partial b_m}\left(\frac{\partial k}{\partial x_j}\right) n_j\, dS - \int_S \varepsilon_a \left(\nu + \frac{\nu_t}{Pr_\varepsilon}\right)\frac{\partial}{\partial b_m}\left(\frac{\partial \varepsilon}{\partial x_j}\right) n_j\, dS \\ &+ \int_{S_w} T_k^1 \frac{\delta x_k}{\delta b_m} dS\end{aligned}$$

or, since in the examined problems, $\frac{\delta J}{\delta b_m}$ is given by Eq. (14),

$$\begin{aligned}\frac{\delta L}{\delta b_m} = &- \int_{S_i} \frac{\partial p}{\partial b_m}\nu_k n_k\, dS - \int_{S_o}\left(\nu_i \frac{\partial \nu_i}{\partial b_m}\nu_k n_k + \frac{1}{2}\nu_i^2 \frac{\partial \nu_k}{\partial b_m} n_k\right) dS + \int_\Omega \left(R_i^u \frac{\partial \nu_i}{\partial b_m} + R^q \frac{\partial p}{\partial b_m} + R^{k_a}\frac{\partial k}{\partial b_m} + R^{\varepsilon_a}\frac{\partial \varepsilon}{\partial b_m}\right) d\Omega \\ &+ \int_S \left(D_i^u \frac{\partial \nu_i}{\partial b_m} + D^q \frac{\partial p}{\partial b_m} + D^{k_a}\frac{\partial k}{\partial b_m} + D^{\varepsilon_a}\frac{\partial \varepsilon}{\partial b_m}\right) dS - \int_S (\nu+\nu_t) u_i \frac{\partial}{\partial b_m}\left(\frac{\partial \nu_i}{\partial x_j} + \frac{\partial \nu_j}{\partial x_i}\right) n_j\, dS \\ &- \int_S k_a \left(\nu + \frac{\nu_t}{Pr_k}\right)\frac{\partial}{\partial b_m}\left(\frac{\partial k}{\partial x_j}\right) n_j\, dS - \int_S \varepsilon_a \left(\nu + \frac{\nu_t}{Pr_\varepsilon}\right)\frac{\partial}{\partial b_m}\left(\frac{\partial \varepsilon}{\partial x_j}\right) n_j\, dS + \int_{S_w} T_k^1 \frac{\delta x_k}{\delta b_m} dS\end{aligned} \tag{17}$$

where $S = S_w \cup S_i \cup S_o$. The last integral is written only along S_w, since $\frac{\delta x_k}{\delta b_m}\Big|_{S_i S_o} = 0$ along the inlet and outlet. The various symbols appearing in Eq. (17) are explained below:

$$R_i^u = -\nu_j\left(\frac{\partial u_j}{\partial x_i} + \frac{\partial u_i}{\partial x_j}\right) - \frac{\partial}{\partial x_j}\left[(\nu+\nu_t)\left(\frac{\partial u_i}{\partial x_j} + \frac{\partial u_j}{\partial x_i}\right)\right] + \frac{\partial q}{\partial x_i} + k_a\frac{\partial k}{\partial x_i} + \varepsilon_a\frac{\partial \varepsilon}{\partial x_i} + 2\frac{\partial}{\partial x_j}\left[\left(k_a + \varepsilon_a c_1 \frac{\varepsilon}{k}\right)\nu_t\left(\frac{\partial \nu_i}{\partial x_j} + \frac{\partial \nu_j}{\partial x_i}\right)\right] \tag{18a}$$

$$R^q = -\frac{\partial u_j}{\partial x_j} \tag{18b}$$

$$\begin{aligned}R^{k_a} = &\, 2c_\mu \frac{k}{\varepsilon}\left(\frac{\partial \nu_i}{\partial x_j} + \frac{\partial \nu_j}{\partial x_i}\right)\frac{\partial u_i}{\partial x_j} - \frac{2}{3}\frac{\partial u_j}{\partial x_j} - \nu_j\frac{\partial k_a}{\partial x_j} - \frac{\partial}{\partial x_j}\left[\left(\nu + \frac{\nu_t}{Pr_k}\right)\frac{\partial k_a}{\partial x_j}\right] + \frac{\partial k_a}{\partial x_j}\frac{2c_\mu}{Pr_k}\frac{\partial k}{\partial x_j}\frac{k}{\varepsilon} - 2k_a c_\mu \frac{k}{\varepsilon}P \\ &+ \frac{\partial \varepsilon_a}{\partial x_j}\frac{2c_\mu}{Pr_\varepsilon}\frac{\partial \varepsilon}{\partial x_j}\frac{k}{\varepsilon} + \varepsilon_a\left(-c_1 c_\mu - c_2\frac{\varepsilon^2}{k^2}\right)P\end{aligned} \tag{18c}$$

$$R^{\varepsilon_a} = -c_\mu\frac{k^2}{\varepsilon^2}\left(\frac{\partial \nu_i}{\partial x_j} + \frac{\partial \nu_j}{\partial x_i}\right)\frac{\partial u_i}{\partial x_j} - \frac{\partial k_a}{\partial x_j}\frac{c_\mu}{Pr_k}\frac{\partial k}{\partial x_j}\frac{k^2}{\varepsilon^2} + k_a c_\mu\frac{k^2}{\varepsilon^2}P + k_a - \nu_j\frac{\partial \varepsilon_a}{\partial x_j} - \frac{\partial}{\partial x_j}\left[\left(\nu + \frac{\nu_t}{Pr_\varepsilon}\right)\frac{\partial \varepsilon_a}{\partial x_j}\right] - \frac{\partial \varepsilon_a}{\partial x_j}\frac{c_\mu}{Pr_\varepsilon}\frac{k^2}{\varepsilon^2}\frac{\partial \varepsilon}{\partial x_j} + 2c_2\frac{\varepsilon}{k}\varepsilon_a \tag{18d}$$

$$D_i^u = u_j\nu_j n_i + u_i\nu_j n_j + (\nu+\nu_t)\left(\frac{\partial u_i}{\partial x_j} + \frac{\partial u_j}{\partial x_i}\right)n_j - q n_i - 2\left(k_a + \varepsilon_a c_1\frac{\varepsilon}{k}\right)\nu_t\left(\frac{\partial \nu_i}{\partial x_j} + \frac{\partial \nu_j}{\partial x_i}\right)n_j \tag{18e}$$

$$D^q = u_j n_j \tag{18f}$$

$$D^{k_a} = -2c_\mu\frac{k}{\varepsilon}\left(\frac{\partial \nu_i}{\partial x_j} + \frac{\partial \nu_j}{\partial x_i}\right)u_i n_j + \frac{2}{3}u_j n_j + \nu_j n_j k_a + \left(\nu + \frac{\nu_t}{Pr_k}\right)\frac{\partial k_a}{\partial x_j}n_j - 2k_a\frac{c_\mu}{Pr_k}\frac{\partial k}{\partial x_j}n_j\frac{k}{\varepsilon} - 2\varepsilon_a\frac{c_\mu}{Pr_\varepsilon}\frac{\partial \varepsilon}{\partial x_j}n_j\frac{k}{\varepsilon} \tag{18g}$$

$$D^{\varepsilon_a} = c_\mu\frac{k^2}{\varepsilon^2}\left(\frac{\partial \nu_i}{\partial x_j} + \frac{\partial \nu_j}{\partial x_i}\right)u_i n_j + k_a\frac{c_\mu}{Pr_k}\frac{\partial k}{\partial x_j}n_j\frac{k^2}{\varepsilon^2} + \nu_j n_j\varepsilon_a + \left(\nu + \frac{\nu_t}{Pr_\varepsilon}\right)\frac{\partial \varepsilon_a}{\partial x_j}n_j + \varepsilon_a\frac{c_\mu}{Pr_\varepsilon}\frac{\partial \varepsilon}{\partial x_j}n_j\frac{k^2}{\varepsilon^2} \tag{18h}$$

$$T_k^1 = (u_i R_i^v + q R^p + k_a R^k + \varepsilon_a R^\varepsilon)n_k \tag{18i}$$

2.4. Field adjoint equations

Starting from Eq. (17), the field mean flow and turbulence adjoint equations are derived by eliminating all field integrals depending on the sensitivities of the mean flow and turbulence variables. Thus, the adjoint to the governing field equations are

$$R_i^u = 0 \tag{19a}$$

$$R^q = 0 \tag{19b}$$

$$R^{k_a} = 0 \tag{19c}$$

$$R^{\varepsilon_a} = 0 \tag{19d}$$

2.5. Inlet conditions

At the inlet, where the nodal coordinates are fixed $\left(\frac{\delta x_i}{\delta b_m}=0\right)$, based on Eq. (12), the imposed Dirichlet conditions on v_i, k and ε imply $\frac{\partial v_i}{\partial b_m}=\frac{\partial k}{\partial b_m}=\frac{\partial \varepsilon}{\partial b_m}=0$; so, the corresponding integrals along S_i in Eq. (17) automatically vanish. In the same equation, integrals that include $\frac{\partial p}{\partial b_m}$ can be eliminated by setting $\int_{S_i}(D^q-v_k n_k)\frac{\partial p}{\partial b_m}dS=0$, which leads to

$$u_i n_i = v_i n_i \tag{20}$$

Eq. (20) states that the normal (to the inlet boundary) primal and adjoint velocity components should be equal. Since the inlet velocity is given, Eq. (20) implies that $u_i\, n_i$ is also known in advance. Next step is to eliminate the integrals including $\frac{\partial}{\partial b_m}\left(\frac{\partial k}{\partial x_i}\right)$ and $\frac{\partial}{\partial b_m}\left(\frac{\partial \varepsilon}{\partial x_i}\right)$, for which it suffices to impose $k_a = \varepsilon_a = 0$ along the inlet boundary. Finally, the last integral along S_i that must vanish is $\int_{S_i}(v+v_t)u_i\frac{\partial}{\partial b_m}\left(\frac{\partial v_i}{\partial x_j}+\frac{\partial v_j}{\partial x_i}\right)n_j\,dS$, alternatively expressed as $\int_{S_i}(v+v_t)(u_k n_k n_i + u_k t_k^l t_i^l)\frac{\partial}{\partial b_m}\left(\frac{\partial v_i}{\partial x_j}+\frac{\partial v_j}{\partial x_i}\right)n_j\,dS$. Since, at the inlet, v_i, n_i and t_i^l remain fixed ($l = 1$ in 2D flows where a single tangential direction exists whereas, in 3D problems, l takes on the values 1 and 2), it can be shown through the use of the continuity equation, that

$$u_k n_k \frac{\partial}{\partial b_m}\left[\left(\frac{\partial v_i}{\partial x_j}n_j\right)n_i+\left(\frac{\partial v_j}{\partial x_i}n_i\right)n_j\right]=2u_k n_k\frac{\partial}{\partial b_m}\left(\frac{\partial v_i}{\partial x_j}n_j n_i\right)=-2u_k n_k\frac{\partial}{\partial b_m}\left(\frac{\partial v_i}{\partial x_j}t_j^l t_i^l\right)=0 \tag{21}$$

Consequently, it suffices to zero the tangential component (s) of the adjoint velocity at the inlet, i.e. $u_i t_i^l = 0$. To sum up, the adjoint velocity vector at the inlet is known, giving rise to Dirichlet conditions for its components u_i.

Thus far, inlet boundary conditions for all the adjoint variables but the adjoint pressure q have been found. Numerical tests proved that a zero Neumann condition may safely be imposed on q. This is compatible with the zero Neumann condition imposed on p along the same boundary. However, since there is no condition derived for q, we are free to impose any other condition on q at the inlet, provided that this does not cause numerical difficulties.

2.6. Outlet conditions

At the outlet, p is given and fixed and $\frac{\partial v_i}{\partial x_j}n_j=\frac{\partial k}{\partial x_j}n_j=\frac{\partial \varepsilon}{\partial x_j}n_j=0$ (due to the zero Neumann conditions imposed on the velocity components, k and ε). Therefore, from the boundary integrals of Eq. (17), written along S_o (instead of S), those which include $\frac{\partial p}{\partial b_m}$, $\frac{\partial}{\partial b_m}\left(\frac{\partial v_i}{\partial x_j}\right)n_j$, $\frac{\partial}{\partial b_m}(\frac{\partial k}{\partial x_j})n_j$ and $\frac{\partial}{\partial b_m}(\frac{\partial \varepsilon}{\partial x_j})n_j$, automatically vanish (recall, n_j does not depend on b_m). To eliminate the integral (along S_o) which includes $\frac{\partial v_i}{\partial b_m}$, the following conditions must be satisfied:

$$-v_i v_k n_k-\frac{1}{2}v_k^2 n_i+D_i^u=0$$

which, due to Eq. (18e), can be written as

$$qn_i-(v+v_t)\left(\frac{\partial u_i}{\partial x_j}+\frac{\partial u_j}{\partial x_i}\right)n_j+2\left(k_a+\varepsilon_a c_1\frac{\varepsilon}{k}\right)v_t\left(\frac{\partial v_i}{\partial x_j}+\frac{\partial v_j}{\partial x_i}\right)n_j-v_j u_j n_i-v_j u_i n_j=-v_i v_k n_k-\frac{1}{2}v_k^2 n_i \tag{22}$$

It is convenient to express Eq. (22) in terms of the normal and tangential components of the adjoint velocity ($u_i\, n_i$ and $u_i t_i^l$, respectively). The following equations can readily be derived

$$u_i t_i^l v_j n_j+(v+v_t)\left(\frac{\partial u_i}{\partial x_j}+\frac{\partial u_j}{\partial x_i}\right)n_j t_i^l-2\left(k_a+\varepsilon_a c_1\frac{\varepsilon}{k}\right)v_t\left(\frac{\partial v_i}{\partial x_j}+\frac{\partial v_j}{\partial x_i}\right)n_j t_i^l=v_i t_i^l v_k n_k \tag{23a}$$

$$u_j v_j+u_i n_i v_j n_j+(v+v_t)\left(\frac{\partial u_i}{\partial x_j}+\frac{\partial u_j}{\partial x_i}\right)n_j n_i-q-2\left(k_a+\varepsilon_a c_1\frac{\varepsilon}{k}\right)v_t\left(\frac{\partial v_i}{\partial x_j}+\frac{\partial v_j}{\partial x_i}\right)n_j n_i=v_i n_i v_k n_k+\frac{1}{2}v_k^2 \tag{23b}$$

Dealing with duct flows, we may easily assume that the outlet boundary is a straight line (2D) or a plane (3D flows). Without loss in generality, we may also assume that, along S_o, the unit normal vector is aligned with the x_1 axis. Such an assumption facilitates the presentation of how the term (in Eq. (17)) that depends on $\frac{\partial}{\partial b_m}\left(\frac{\partial v_i}{\partial x_j}+\frac{\partial v_j}{\partial x_i}\right)n_j$ or only $\frac{\partial}{\partial b_m}(\frac{\partial v_j}{\partial x_i})n_j$ since $\frac{\partial v_i}{\partial x_j}n_j=0$, can be eliminated. For a straight or plane boundary, either this is automatically zeroed (on condition that there is uniform flow at the outlet, i.e. without the presence of a solid wall and the boundary layer developed along it) or the conditions

$$u_i t_i^l = 0 \tag{24}$$

must be imposed.

One may use Eqs. (23) in more than one ways, depending on whether Eq. (24) must also be satisfied or not. One may solve Eq. (23a) for the tangential adjoint velocity $u_i t_i^l$ and Eq. (23b) for the adjoint pressure q. In such a case, any condition could be imposed on the normal adjoint velocity $u_i\, n_i$. Alternatively, one may arbitrarily set $q = 0$ along the outlet and, then, solve Eqs. (23a) and (23b) for $u_i t_i^l$ and $u_i\, n_i$, respectively. Both approaches have been programmed and tested, among other, on the cases examined in the Case Studies section. Even in the case $\frac{\partial}{\partial b_m}(\frac{\partial v_j}{\partial x_i}n_j)\neq 0$, they produced practically identical results (i.e. sensitivity derivatives). In case Eq. (24) should be satisfied, the outlet tangential adjoint velocity is set to zero, Eq. (23a) is then solved

for $\frac{\partial u_i}{\partial x_j} n_i t_j^l$ (which, through integration and after defining arbitrarily the $u_i\, n_i$ value at one point along S_o, gives the $u_i\, n_i$ values over the outlet) and finally, Eq. (23b) is solved for the adjoint pressure q. This third outlet boundary condition scenario led also to the same results as before.

Finally, the elimination of the integrals along S_o which depend on $\frac{\partial k}{\partial b_m}$ and $\frac{\partial \varepsilon}{\partial b_m}$ in Eq. (17), makes it necessary to impose

$$D^{k_a} = 0, \quad D^{\varepsilon_a} = 0$$

along the outlet. By using Eqs. (18g) and (18h), we get

$$-2c_\mu \frac{k}{\varepsilon}\left(\frac{\partial v_i}{\partial x_j} + \frac{\partial v_j}{\partial x_i}\right) u_i n_j + \frac{2}{3} u_j n_j + v_j n_j k_a + \left(v + \frac{v_t}{Pr_k}\right)\frac{\partial k_a}{\partial x_j} n_j = 0 \tag{25a}$$

$$c_\mu \frac{k^2}{\varepsilon^2}\left(\frac{\partial v_i}{\partial x_j} + \frac{\partial v_j}{\partial x_i}\right) u_i n_j + v_j n_j \varepsilon_a + \left(v + \frac{v_t}{Pr_\varepsilon}\right)\frac{\partial \varepsilon_a}{\partial x_j} n_j = 0 \tag{25b}$$

Eq. (25a) can be solved for k_a (with frozen $\frac{\partial k_a}{\partial x_j} n_j$, computed using the current k_a field) and Eq. (25b) for ε_a (with frozen $\frac{\partial \varepsilon_a}{\partial x_j} n_j$), during the iterative solution of the adjoint turbulence variable equations.

It is also helpful to associate the outlet adjoint boundary conditions with the finite volume discretization scheme at the outlet nodes. Let Ω_P be the finite volume centered at an outlet node P and surrounded by its boundary S_P. The latter comprises segments lying in the interior of the flow domain and, also, segment $\alpha\beta$ lying along the outlet boundary, Fig. 1. The integration of the adjoint momentum equations $R_i^u = 0$ (where R_i^u are given by Eq. (18a)) over Ω_P leads to

$$\int_{S_P} \left[q n_i - (v + v_t)\left(\frac{\partial u_i}{\partial x_j} + \frac{\partial u_j}{\partial x_i}\right) n_j + 2\left(k_a + \varepsilon_a c_1 \frac{\varepsilon}{k}\right) v_t \left(\frac{\partial v_i}{\partial x_j} + \frac{\partial v_j}{\partial x_i}\right) n_j - v_j u_j n_i - v_j u_i n_j \right] dS$$
$$+ \int_{\Omega_P} \left(u_j \frac{\partial v_j}{\partial x_i} + k_a \frac{\partial k}{\partial x_i} + \varepsilon_a \frac{\partial \varepsilon}{\partial x_i} \right) d\Omega = 0 \tag{26}$$

It is straightforward to rewrite Eq. (26), by replacing the part of its first integral written along $\alpha\beta$, i.e. $\int_{\alpha\beta}[q n_i - (v + v_t)\left(\frac{\partial u_i}{\partial x_j} + \frac{\partial u_j}{\partial x_i}\right) n_j + 2\left(k_a + \varepsilon_a c_1 \frac{\varepsilon}{k}\right) v_t \left(\frac{\partial v_i}{\partial x_j} + \frac{\partial v_j}{\partial x_i}\right) n_j - v_j u_j n_i - v_j u_i n_j] dS$, by $\int_{\alpha\beta} \left(-v_i v_k n_k - \frac{1}{2} v_k^2 n_i\right) dS$. Based on the equation above, it seems that, according to the finite volume scheme used, all integrals along the outlet $\alpha\beta$ segment depend exclusively on the known velocity field.

2.7. "Wall" conditions

At the "wall" boundary, in order to make $\frac{\delta L}{\delta b_m}$ (Eq. (17)) independent of $\frac{\partial}{\partial b_m}\left(\frac{\partial k}{\partial x_j}\right)$ and $\frac{\partial}{\partial b_m}\left(\frac{\partial \varepsilon}{\partial x_j}\right)$, the adjoint turbulent variables should be zeroed, $k_a = \varepsilon_a = 0$. For $\frac{\delta L}{\delta b_m}$ to be independent of $\frac{\partial p}{\partial b_m}$, the adjoint no-penetration condition $u_i\, n_i = 0$ must be met. The remaining terms provide the adjoint flux (es) at the "wall" and the sensitivity derivatives, as follows:

$$\frac{\delta L}{\delta b_m} = \int_{S_w} \left(D_i^u \frac{\partial v_i}{\partial b_m} + D^{k_a} \frac{\partial k}{\partial b_m} + D^{\varepsilon_a} \frac{\partial \varepsilon}{\partial b_m} \right) dS - \int_{S_w} (v + v_t) u_i \frac{\partial}{\partial b_m}\left(\frac{\partial v_i}{\partial x_j} + \frac{\partial v_j}{\partial x_i}\right) n_j\, dS + \int_{S_w} T_k^1 \frac{\delta x_k}{\delta b_m} dS \tag{27}$$

It can be shown that

$$(v + v_t) u_i \frac{\partial}{\partial b_m}\left(\frac{\partial v_i}{\partial x_j} + \frac{\partial v_j}{\partial x_i}\right) n_j\, dS = T^3 \frac{\delta v_\tau}{\delta b_m} + T_i^4 \frac{\delta n_i}{\delta b_m} + T_i^5 \frac{\delta t_i^l}{\delta b_m} + T_k^2 \frac{\delta x_k}{\delta b_m} \tag{28}$$

where

$$T^3 = u_k t_k^l \left[2 v_\tau + \frac{v_\tau^2}{v + v_t} c_\mu \frac{k}{\varepsilon}\left(\frac{k}{\varepsilon} \frac{\delta \varepsilon}{\delta v_\tau} - 2 \frac{\delta k}{\delta v_\tau} \right) \right]$$
$$T_i^4 = -u_k t_k^l (v + v_t)\left(\frac{\partial v_i}{\partial x_j} + \frac{\partial v_j}{\partial x_i}\right) t_j^l$$
$$T_i^5 = -u_k t_k^l (v + v_t)\left(\frac{\partial v_i}{\partial x_j} + \frac{\partial v_j}{\partial x_i}\right) n_j$$
$$T_k^2 = -(v + v_t) u_q t_q^l t_i^l n_j \left(\frac{\partial^2 v_i}{\partial x_j \partial x_k} + \frac{\partial^2 v_j}{\partial x_i \partial x_k} \right) \tag{29}$$

while $\frac{\delta k}{\delta v_\tau}$ and $\frac{\delta \varepsilon}{\delta v_\tau}$ are deduced from Eq. (8).

To handle the term in Eq. (27) that depends on $\frac{\partial v_i}{\partial b_m}$ along the "wall", the no-penetration condition for the primal velocity ($v_i\, n_i = 0$) and the law of the wall (Eq. (7)) should be taken into account, leading to

$$D_i^u \frac{\partial v_i}{\partial b_m} = T^6 \frac{\delta v_\tau}{\delta b_m} + T_i^7 \frac{\delta t_i^l}{\delta b_m} + T_k^8 \frac{\delta x_k}{\delta b_m} \tag{30}$$

where

$$T^6 = D_i^u t_i^l c_v, \quad T_i^7 = D_i^u v_k t_k^l, \quad T_k^8 = -D_i^u \frac{\partial v_i}{\partial x_k} \tag{31}$$

and

$$c_\nu = \begin{cases} \frac{1}{\kappa} ln y^+ + B + \frac{1}{\kappa}, & y^+ \geqslant y_c^+ \\ \frac{2\nu_\tau \Delta}{\nu}, & y^+ < y_c^+ \end{cases} \tag{32}$$

Boundary integrals in Eq. (27) that depend on $\frac{\partial k}{\partial b_m}$ and $\frac{\partial \varepsilon}{\partial b_m}$ are handled in a similar way, resulting to the expressions

$$\begin{aligned} D^{k_a} \frac{\partial k}{\partial b_m} &= T^9 \frac{\delta \nu_\tau}{\delta b_m} + T_k^{10} \frac{\delta x_k}{\delta b_m} \\ D^{\varepsilon_a} \frac{\partial \varepsilon}{\partial b_m} &= T^{11} \frac{\delta \nu_\tau}{\delta b_m} + T_k^{12} \frac{\delta x_k}{\delta b_m} \end{aligned} \tag{33}$$

where

$$T^9 = D^{k_a} \frac{\delta k}{\delta \nu_\tau}, \quad T_k^{10} = -D^{k_a} \frac{\partial k}{\partial x_k}, \quad T^{11} = D^{\varepsilon_a} \frac{\delta \varepsilon}{\delta \nu_\tau}, \quad T_k^{12} = -D^{\varepsilon_a} \frac{\partial \varepsilon}{\partial x_k} \tag{34}$$

Eq. (27) is rewritten as

$$\frac{\delta L}{\delta b_m} = \int_{S_w} (T^6 + T^9 + T^{11} + T^3) \frac{\delta \nu_\tau}{\delta b_m} dS + \int_{S_w} \left(T_i^7 + T_i^5 \right) \frac{\delta t_i^l}{\delta b_m} dS + \int_{S_w} T_i^4 \frac{\delta n_i}{\delta b_m} dS + \int_{S_w} (T_k^8 + T_k^{10} + T_k^{12} + T_k^2 + T_k^1) \frac{\delta x_k}{\delta b_m} dS \tag{35}$$

Since the sensitivity derivatives must be independent of $\frac{\delta \nu_\tau}{\delta b_m}$, according to Eq. (35), the condition

$$T^6 + T^9 + T^{11} + T^3 = 0 \tag{36}$$

should hold. Similar to the wall function technique and the definition of the friction velocity ν_τ, (Eq. (6)), the adjoint friction velocity associated with each "wall" grid node is defined by

$$u_\tau^2 = (\nu + \nu_t) \left(\frac{\partial u_i}{\partial x_j} + \frac{\partial u_j}{\partial x_i} \right) n_j t_i \tag{37}$$

Thus, condition (36) leads to

$$u_\tau^2 = \frac{1}{c_\nu} \left[2 u_k t_k \nu_\tau - \left(\nu + \frac{\nu_t}{Pr_k} \right) \frac{\partial k_a}{\partial x_j} n_j \frac{\delta k}{\delta \nu_\tau} - \left(\nu + \frac{\nu_t}{Pr_\varepsilon} \right) \frac{\partial \varepsilon_a}{\partial x_j} n_j \frac{\delta \varepsilon}{\delta \nu_\tau} \right] \tag{38}$$

which is used to compute the adjoint viscous fluxes at the "wall" nodes.

2.8. Sensitivity derivatives

By satisfying condition (38), the first integral in Eq. (35) vanishes and the remaining terms give the sensitivity derivatives

$$\begin{aligned} \frac{\delta L}{\delta b_m} = & \int_{S_w} \left[(\nu + \nu_t) \left(\frac{\partial u_i}{\partial x_j} + \frac{\partial u_j}{\partial x_i} \right) n_j - q n_i \right] \left(\nu_k t_k^l \frac{\delta t_i^l}{\delta b_m} - \frac{\partial \nu_i}{\partial x_k} \frac{\delta x_k}{\delta b_m} \right) dS \\ & + \int_{S_w} (\nu + \nu_t) \left[u_k t_k^l \left(\frac{\partial \nu_i}{\partial x_j} + \frac{\partial \nu_j}{\partial x_i} \right) \frac{\delta (n_j t_i^l)}{\delta b_m} + u_q t_q^l \left(\frac{\partial^2 \nu_i}{\partial x_j \partial x_k} + \frac{\partial^2 \nu_j}{\partial x_i \partial x_k} \right) \frac{\delta x_k}{\delta b_m} n_j t_i^l \right] dS \\ & - \int_{S_w} \left[-2 c_\mu \frac{k}{\varepsilon} \left(\frac{\partial \nu_i}{\partial x_j} + \frac{\partial \nu_j}{\partial x_i} \right) u_i n_j + \left(\nu + \frac{\nu_t}{Pr_k} \right) \frac{\partial k_a}{\partial x_j} n_j \right] \frac{\partial k}{\partial x_k} \frac{\delta x_k}{\delta b_m} dS \\ & - \int_{S_w} \left[c_\mu \frac{k^2}{\varepsilon^2} \left(\frac{\partial \nu_i}{\partial x_j} + \frac{\partial \nu_j}{\partial x_i} \right) u_i n_j + \left(\nu + \frac{\nu_t}{Pr_\varepsilon} \right) \frac{\partial \varepsilon_a}{\partial x_j} n_j \right] \frac{\partial \varepsilon}{\partial x_k} \frac{\delta x_k}{\delta b_m} dS + \int_{S_w} u_i R_i^\nu \frac{\delta x_k}{\delta b_m} n_k \, dS + \int_{S_w} q R^p \frac{\delta x_k}{\delta b_m} n_k \, d\Omega \end{aligned} \tag{39}$$

Further processing of Eq. (39) reduces the order of the spatial derivatives to be computed. The last two integrals can be written as

$$\begin{aligned} \int_{S_w} u_i R_i^\nu \frac{\delta x_k}{\delta b_m} n_k \, dS = & \int_{S_w} u_i \nu_j \frac{\partial \nu_i}{\partial x_j} \frac{\delta x_k}{\delta b_m} n_k \, dS + \int_{S_w} u_i \frac{\partial p_{eff}}{\partial x_i} \frac{\delta x_k}{\delta b_m} n_k \, dS - \int_{S_w} (\nu + \nu_t) u_i \frac{\partial}{\partial x_j} \left(\frac{\partial \nu_i}{\partial x_j} + \frac{\partial \nu_j}{\partial x_i} \right) \frac{\delta x_k}{\delta b_m} n_k \, dS \\ & - \int_{S_w} 2 c_\mu \frac{k}{\varepsilon} \frac{\partial k}{\partial x_j} \left(\frac{\partial \nu_i}{\partial x_j} + \frac{\partial \nu_j}{\partial x_i} \right) u_i \frac{\delta x_k}{\delta b_m} n_k \, dS + \int_{S_w} c_\mu \frac{k^2}{\varepsilon^2} \frac{\partial \varepsilon}{\partial x_j} \left(\frac{\partial \nu_i}{\partial x_j} + \frac{\partial \nu_j}{\partial x_i} \right) u_i \frac{\delta x_k}{\delta b_m} n_k \, dS \end{aligned} \tag{40}$$

and

$$\int_{S_w} q R^p \frac{\delta x_k}{\delta b_m} n_k \, dS = \int_{S_w} q \frac{\partial \nu_i}{\partial x_i} \frac{\delta x_k}{\delta b_m} n_k \, dS \tag{41}$$

By substituting Eqs. (40) and (41) into Eq. (39) and rearranging, one gets

$$\begin{aligned}\frac{\delta L}{\delta b_m} &= \int_{S_w}\left[(\nu+\nu_t)\left(\frac{\partial u_i}{\partial x_j}+\frac{\partial u_j}{\partial x_i}\right)n_j\right]\left(\nu_k t_k^l\frac{\delta t_i^l}{\delta b_m}-\frac{\partial v_i}{\partial x_k}\frac{\delta x_k}{\delta b_m}\right)dS-\int_{S_w} q\nu_k t_k^l n_i\frac{\delta t_i^l}{\delta b_m}dS\\ &+\int_{S_w}(\nu+\nu_t)u_k t_k^l\left(\frac{\partial v_i}{\partial x_j}+\frac{\partial v_j}{\partial x_i}\right)\frac{\delta(n_j t_i^l)}{\delta b_m}dS-\int_{S_w}(\nu+\nu_t)u_k t_k^l t_j^l L_i^{(m)}\left(\frac{\partial v_i}{\partial x_j}+\frac{\partial v_j}{\partial x_i}\right)dS-\int_{S_w}\left(\nu+\frac{\nu_t}{Pr_k}\right)\frac{\partial k_a}{\partial x_j}n_j\frac{\partial k}{\partial x_k}\frac{\delta x_k}{\delta b_m}dS\\ &+\int_{S_w}\left(\nu+\frac{\nu_t}{Pr_\varepsilon}\right)\frac{\partial \varepsilon_a}{\partial x_j}n_j\frac{\partial \varepsilon}{\partial x_k}\frac{\delta x_k}{\delta b_m}dS-\int_{S_w}2c_\mu\frac{k}{\varepsilon}u_j\left(\frac{\partial v_i}{\partial x_j}+\frac{\partial v_j}{\partial x_i}\right)L_i^{(m)}(k)dS+\int_{S_w}c_\mu\frac{k^2}{\varepsilon^2}u_j\left(\frac{\partial v_i}{\partial x_j}+\frac{\partial v_j}{\partial x_i}\right)L_i^{(m)}(\varepsilon)dS\\ &\times\int_{S_w}v_i u_j L_i^{(m)}(v_j)dS+\int_{S_w}u_i L_i^{(m)}(p)dS-\int_{S_w}qL_i^{(m)}(v_i)dS\end{aligned}\tag{42}$$

where the operator $L_i^{(m)}()$ is defined by

$$L_i^{(m)}()\equiv\frac{\partial()}{\partial x_i}\frac{\delta x_k}{\delta b_m}n_k-\frac{\partial()}{\partial x_k}\frac{\delta x_k}{\delta b_m}n_i\tag{43}$$

or

$$L_i^{(m)}()=\frac{\partial()}{\partial x_k}t_k^l(n_j t_i^l-t_j^l n_i)\frac{\delta x_j}{\delta b_m}\tag{44}$$

Eq. (44) expresses the $L_i^{(m)}()$ operator, applied to any scalar quantity, as the product of its tangential derivative along the "wall" $\frac{\partial()}{\partial t}$ and the quantity $(n_j t_i^l-t_j^l n_i)\frac{\delta x_j}{\delta b_m}$. In a 2*D* case, for instance, using $\boldsymbol{n}$ and $\boldsymbol{t}$ (where $\boldsymbol{n}$ is the unit normal vector which is perpendicular to the "wall" and points away from the flow region bounded by S_w and $\boldsymbol{t}$ is the tangential unit vector), it can be shown that

$$L_1^{(m)}()=\frac{\partial()}{\partial t}\frac{\delta x_2}{\delta b_m},\quad L_2^{(m)}()=-\frac{\partial()}{\partial t}\frac{\delta x_1}{\delta b_m}\tag{45}$$

It is evident that, using Eq. (45) in (42), the computational accuracy increases noticeably; the majority of the computations are based on the integration of the tangential derivatives along the wall. This is absolutely clear for the three last integrals in Eq. (42); using Eq. (45), the integration of terms involving $\frac{\partial v_i}{\partial t}$ or $\frac{\partial p}{\partial t}$ is due.

Also, using Eq. (8) (if $y^+\geqslant y_c^+$), we may write

$$\int_{S_w}\left[-2c_\mu\frac{k}{\varepsilon}u_j L_i^{(m)}(k)+c_\mu\frac{k^2}{\varepsilon^2}u_j L_i^{(m)}(\varepsilon)\right]\left(\frac{\partial v_i}{\partial x_j}+\frac{\partial v_j}{\partial x_i}\right)dS=-\int_{S_w}\kappa\Delta\frac{\partial v_\tau}{\partial t}\left(\frac{\delta x_2}{\delta b_m}-\frac{\delta x_1}{\delta b_m}\right)\left(\frac{\partial v_i}{\partial x_j}+\frac{\partial v_j}{\partial x_i}\right)dS\tag{46}$$

which can also be computed with accuracy by integrating quantities computed along the "wall".

The previous analysis of some indicative terms from Eq. (42) demonstrates that, using Eq. (44), the sensitivity derivatives are computed with excellent numerical accuracy.

3. Case studies

To assess the accuracy of the computed sensitivity derivatives, two duct flow cases are studied. In each case, the sensitivity derivatives computed by the present method are compared with those by finite differences. The objective function is the one given in Eq. (1). Since the accuracy with which the sensitivity derivatives are computed is of key importance in this paper, it should become clear that the state (mean flow and turbulence) equations presented in Section 2 along with the grid and the numerical scheme used are considered to provide "accurate" flow fields. Consequently, sensitivity derivatives computed by finite differences with calls to the aforementioned flow solver are used as reference values, for the purpose of validation. Then, once the search direction has been computed by the proposed method, a steepest descent algorithm is used to optimize the duct shapes for minimum total pressure losses, at predefined flow conditions. Note that any other gradient-based algorithm (such as a quasi-Newton method) could be used instead. It is beyond the scope of this paper to compare the various descent algorithms and the ensuing discussion focuses on the accuracy of the computed derivatives.

For the first case, an axial diffuser (divergent duct) is considered. Even if we aim at designing a symmetrical duct and the starting geometry is symmetrical too, the whole duct is modeled without resorting to symmetry conditions. Only its lower wall is parameterized; the upper one is mirrored. The flow is turbulent with Reynolds number based on the inlet duct height equal to $Re = 1\times10^6$. Unstructured grids are used with 8895 nodes and 17264 triangular elements. The non-dimensional distance of the first nodes off the wall is well above unit (average value of the order of 100). The part of the solid wall shape to be optimized is parameterized using five Bézier control points. The upstream and downstream extensions of the flow domain are not affected by the parameterization and so do the inlet and outlet cross-sections. Hence, the boundary nodes along the straight wall extensions and the inlet/outlet straight segments are fixed. The variables b_m, with respect to which the sensitivity derivatives of the objective function are computed, are the x and y coordinates of all but the first and last Bézier control points of each side.

Each flow solution costs about 5 min in a 64 bit, Quad Core Xeon processor when each adjoint solutions cost ~5.6 min. Though, usually, the computational cost of the adjoint solution is slightly less than that of the flow solution (about 80–90%) due to the linearity of the latter, the present adjoint code is slightly more expensive since the adjoint boundary condition at the wall (adjoint friction velocity) is more complex. Thus, the computational cost of the adjoint approach was

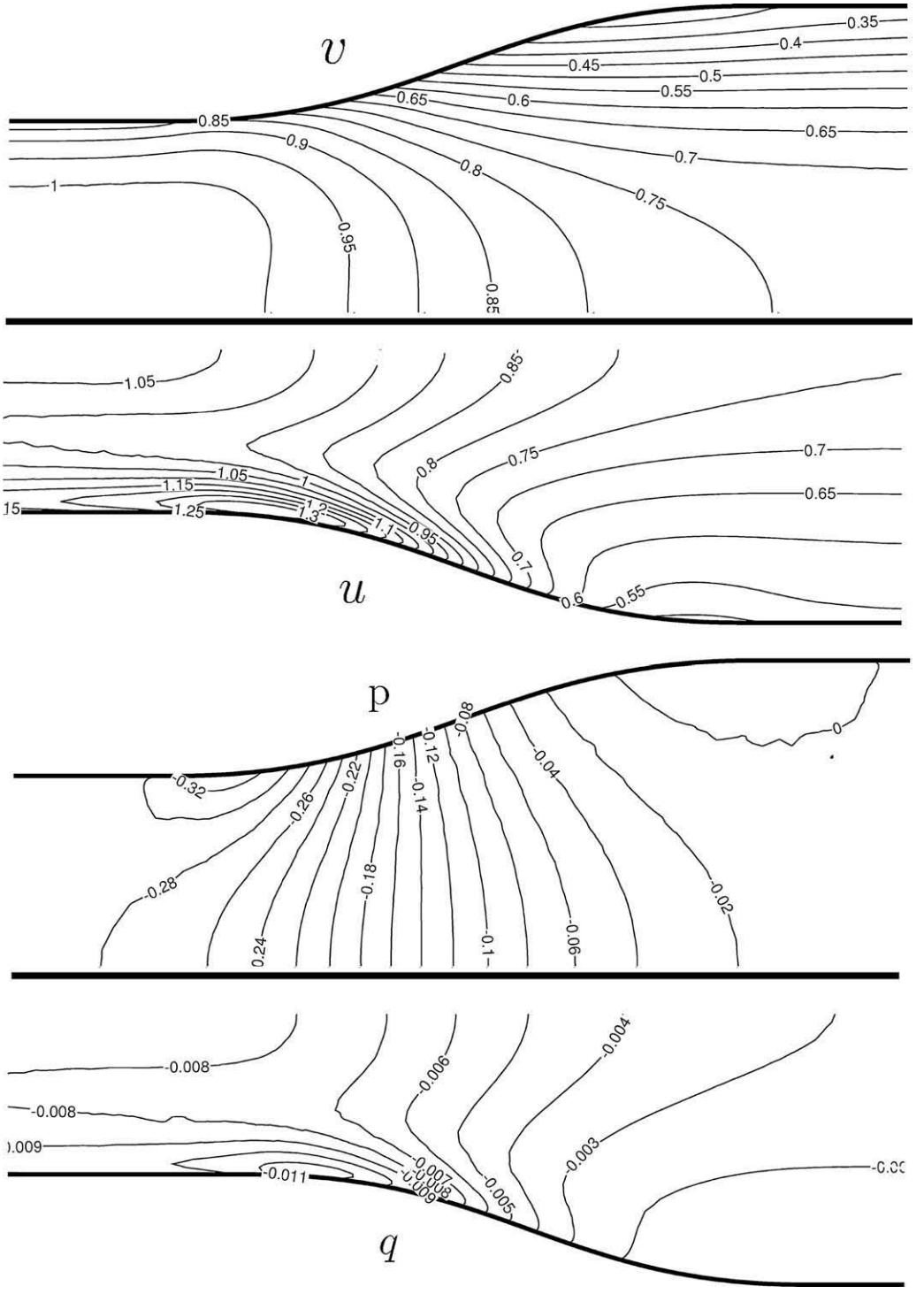

Fig. 2. Axial diffuser, starting shape. (Top) Primal (upper half) and adjoint (lower half) velocity magnitude $|v|$ contours. (Bottom) Primal (top half) and adjoint (lower half) pressure p contours.

now ~110% of the cost for the flow solution. The flow equations were converged by almost 12 orders of magnitude using a point-implicit Jacobi solver.

In Fig. 2, a close-up view of the primal and adjoint velocity magnitude and pressure contours at the divergent part of the starting symmetrical duct geometry are shown. The flow remains attached, allowing the use of wall functions for its modeling. The velocity is decreased along the length of the diffuser and so does the adjoint velocity. Since the static pressure is increased, the adjoint pressure is increased too. The distribution of the adjoint wall stress, expressed by the (squared) adjoint friction velocity u_τ^2 along the divergent part of the duct can be seen in Fig. 3 along with that of the primal friction velocity v_τ. A useful observation concerning the role of Eq. (38) can be gleaned from the comparison of these two distributions. For the sake of convenience, Eq. (38), which is rich with meaning, can be written as $u_\tau^2 = f(u_k t_k^l)$, by ignoring the last two terms including $\frac{\delta k}{\delta v_\tau}$ and $\frac{\delta \varepsilon}{\delta v_\tau}$. This simplification, which was not used during the numerical computations, can be ascertained by the examination of the numerical results. Given that the tangent to the wall adjoint velocity $u_k\ t_k$ is only slightly reduced in the divergent part (recall the application of slip conditions along the "walls"), u_τ^2 remains almost proportional to v_τ and this can clearly be seen in Fig. 2. Both friction velocities are decreased in a similar manner, reflecting the flow deceleration.

In Fig. 4, the contours of k, k_a, ε and ε_a along the divergent part of the diffuser are plotted. One may see the "usual" peaks in the k and ε fields close to the end of the divergent part of the duct, associated with peaks in the adjoint k_a and ε_a values upstream, i.e. close to the start of diffusion. The normal to the wall distributions of the adjoint turbulence variables at several positions along the duct walls are shown in Fig. 5. In this figure, the adjoints k_a and ε_a bear high values in the proximity of the wall and resemble to the k and ε behavior in this region.

For a given diffuser shape, which is then used as the starting shape during the optimization, the sensitivity derivatives of J with respect to the six design variables b_m, computed using the proposed adjoint approach and finite differences, are shown and compared in Fig. 6 and Table 1.

The comparisons prove that the sensitivity derivatives computed by the proposed adjoint approach are very close to the finite difference values. Small deviations exist only at the design variables with respect to which the objective function is rather insensitive (i.e. the corresponding sensitivity derivatives take on small values). To prove the necessity of the complete adjoint approach to the wall functions, an incomplete adjoint formulation was also set up. Based on the state equations, the mean flow and the turbulence model equations are strongly coupled through the law of the wall. For this reason, building an incomplete adjoint method is not straightforward as, for instance, is the "frozen turbulence" assumption in case a low-Reynolds turbulence model is in use. In our case, the incomplete approach assumed that k, ε and v_τ (not, however, v_i) are invariant with respect to the design variables. The sensitivity derivative values computed using the incomplete adjoint approach are shown in Table 1 (marked with FT) and differ noticeably from those computed by the complete adjoint method.

Also, due to the fact that the finite-differences approach is well known for its sensitivity with respect to the selected step size (eps) value a relevant investigation is shown in Table 2. The conclusion drawn is that the computed sensitivity derivatives (as in Table 1, marked with FD) are independent of the step size value and, thus, absolutely dependable.

As mentioned above, the six design variables correspond to the coordinates of the three internal Bézier control points (denoted by *CP*1, *CP*2 and *CP*3, numbered from the left along the x axis, Fig. 6). Several comments can be made on the sign and value of each derivatives which are all in accordance with our qualitative expectations. For instance, if the *CP1.x* value is increased (i.e. *CP*1 moves in the positive x-direction, see Fig. 8), the steepness of the duct wall becomes pronounced and the viscous losses are increased too. This clearly explains the positive sign of the first sensitivity derivative in Fig. 6. Just in the

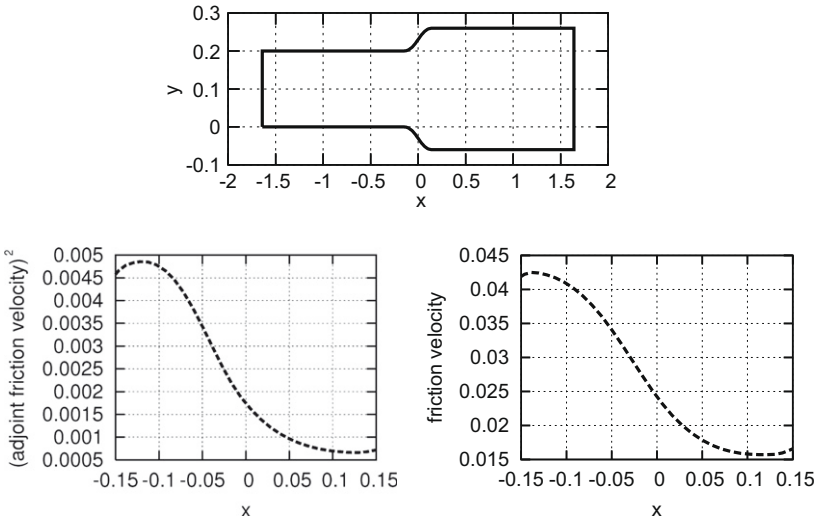

Fig. 3. Axial diffuser, starting shape (not in scale). (Left) Squared adjoint friction velocity u_τ^2 distribution. (Right) Primal friction velocity v_τ distribution.

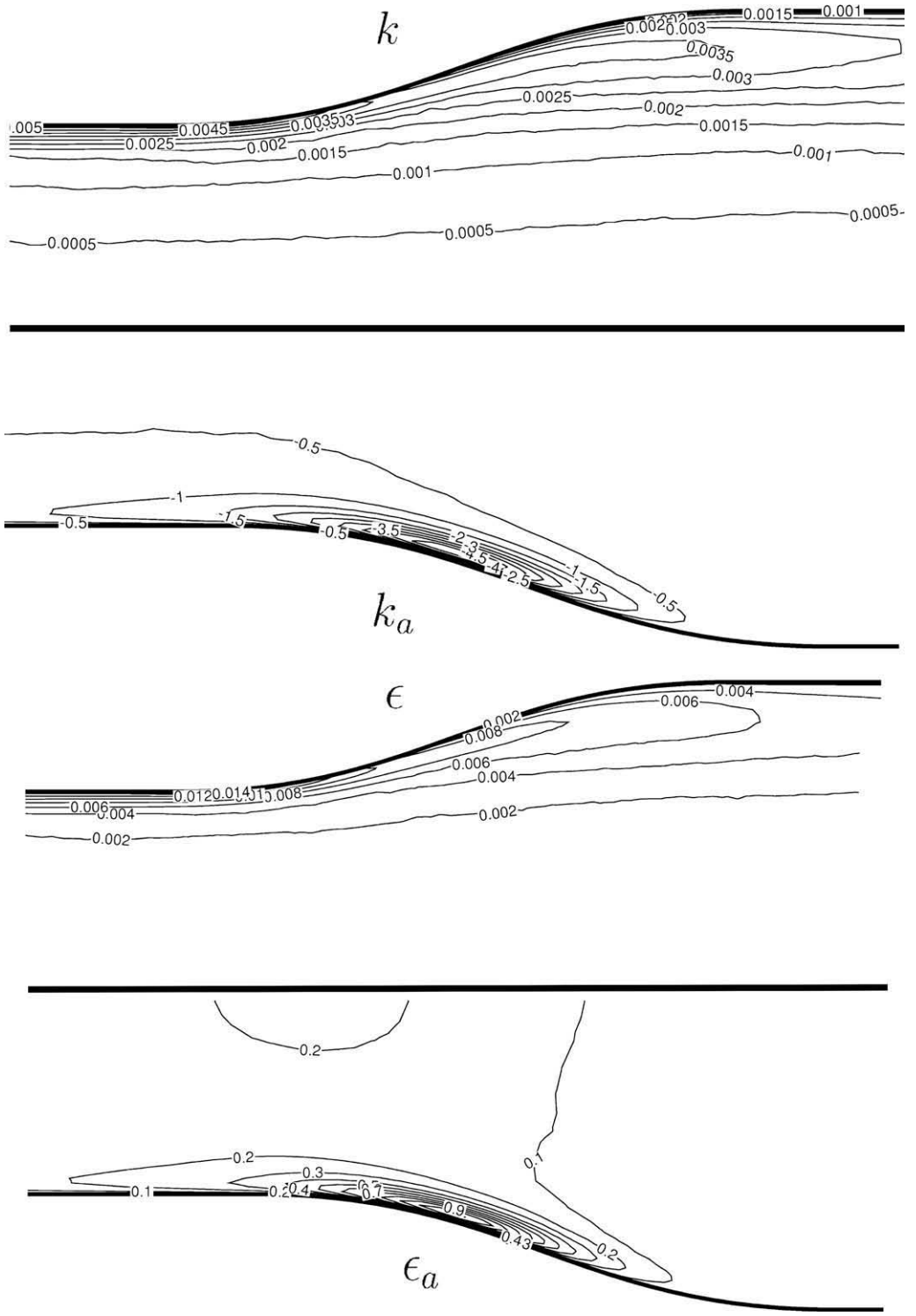

Fig. 4. Axial diffuser, starting shape. (Top) Primal k (upper half) and the adjoint k_a (lower half) contours. Bottom: primal ε (top-half) and the adjoint ε_a (lower half) contours.

opposite way, a small increase in *CP*3.*x* results to locally milder diffusion and less losses; this agrees perfectly with the negative sign of the third derivative. Also, increasing the value of *CP*1.*y* is another way of making the duct steeper in its front part and certainly explains the positive sign of the fourth sensitivity derivative. As far as *CP*3.*y* is of concern, this corresponds to a

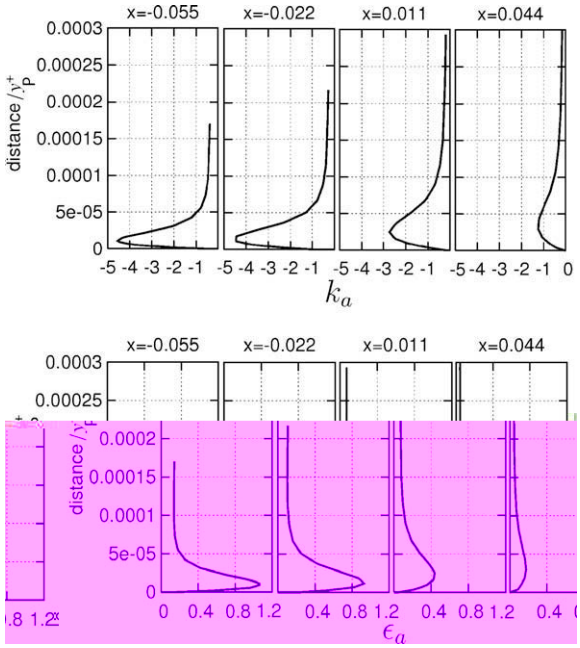

Fig. 5. Axial diffuser, starting shape. Adjoint k_a (top) and ε_a (bottom) normal to the wall distributions at four different positions along the divergent part of the lower wall.

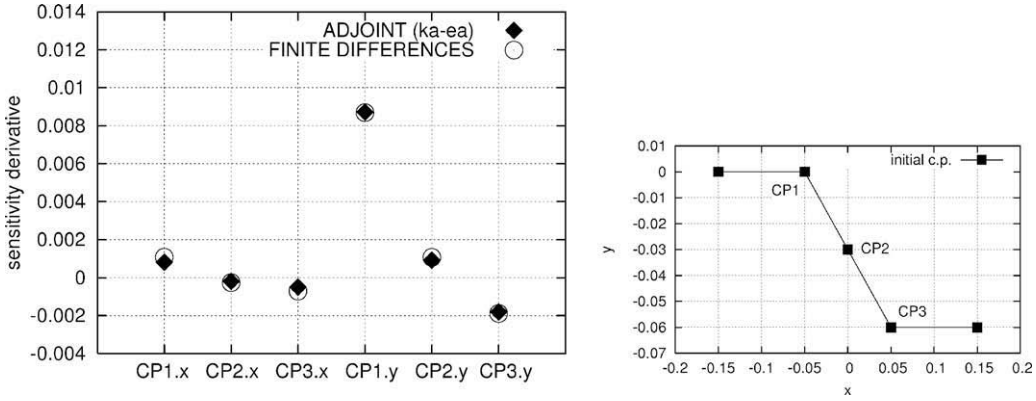

Fig. 6. Axial diffuser, starting shape. Sensitivity derivatives (left) with respect to the design variables (right).

Table 1
Axial diffuser: sensitivity derivative values computed using the proposed adjoint approach (AV), the adjoint approach with frozen turbulence (FT) and finite differences with $eps = 10^{-5}$ (FD).

	$\frac{\delta F}{\delta b_1}10^3$	$\frac{\delta F}{\delta b_2}10^3$	$\frac{\delta F}{\delta b_3}10^3$	$\frac{\delta F}{\delta b_4}10^3$	$\frac{\delta F}{\delta b_5}10^3$	$\frac{\delta F}{\delta b_6}10^3$
AV	0.809111	−0.193240	−0.494843	8.715816	0.920189	−1.804938
FT	0.368930	−0.480133	−0.481642	1.565383	−1.720387	−1.680488
FD	1.079481	−0.260322	−0.708775	8.684181	1.067217	−1.888245

negative derivative value since, by increasing *CP*3.*y*, losses are expected to decrease. Finally, the second free Bézier control point has almost neutral behavior (i.e. it is almost insignificant for this particular diffuser shape) as one may easily guess by examining Fig. 8.

Using the proposed method for the computation of exact sensitivity derivatives, an optimization procedure based on the steepest descent method is carried out and its performance is shown in Fig. 7. The starting and final (deduced upon completion of the optimization loop) duct shapes are illustrated in Fig. 8 along with the corresponding Bézier control points. As expected, the optimal shape has a milder wall slope.

Table 2
Axial diffuser: sensitivity derivative values computed using finite differences with different values of the step size eps.

eps	$\frac{\delta F}{\delta b_1}10^3$	$\frac{\delta F}{\delta b_2}10^3$	$\frac{\delta F}{\delta b_3}10^3$	$\frac{\delta F}{\delta b_4}10^3$	$\frac{\delta F}{\delta b_5}10^3$	$\frac{\delta F}{\delta b_6}10^3$
10^{-3}	1.079663	−0.260377	−0.708893	8.735602	1.076892	−1.886743
10^{-4}	1.079481	−0.260326	−0.708780	8.684572	1.067312	−1.888232
10^{-5}	1.079481	−0.260322	−0.708775	8.684181	1.067217	−1.888245
10^{-6}	1.079481	−0.260322	−0.708776	8.684176	1.067216	−1.888246
10^{-7}	1.079481	−0.260321	−0.708776	8.684176	1.067217	−1.888245
10^{-8}	1.079480	−0.260315	−0.708758	8.684188	1.067220	−1.888238
10^{-9}	1.079733	−0.260236	−0.708880	8.684050	1.066874	−1.888362
10^{-10}	1.080321	−0.260508	−0.708773	8.684650	1.065857	−1.888672

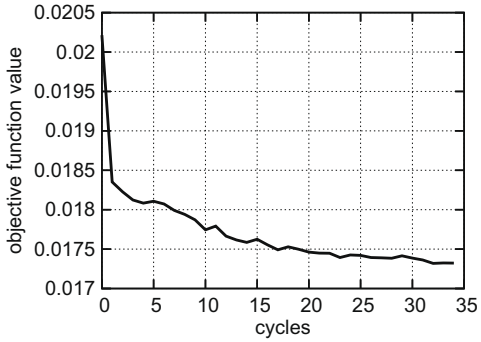

Fig. 7. Axial diffuser. Reduction of the objective function value (total pressure losses between the inlet and the outlet) during the optimization cycles.

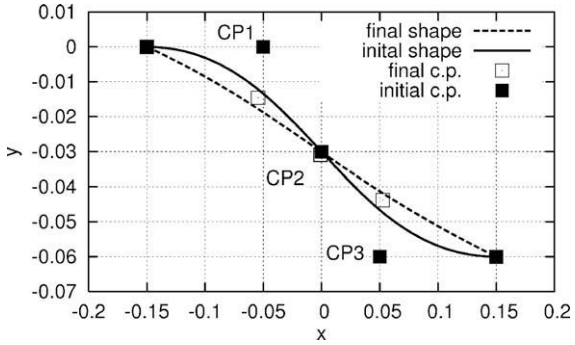

Fig. 8. Axial diffuser. The starting and final lower wall shapes in enlarged scale ordinate axis to highlight the modification in shape. The corresponding Bézier design variables of each shape are also presented.

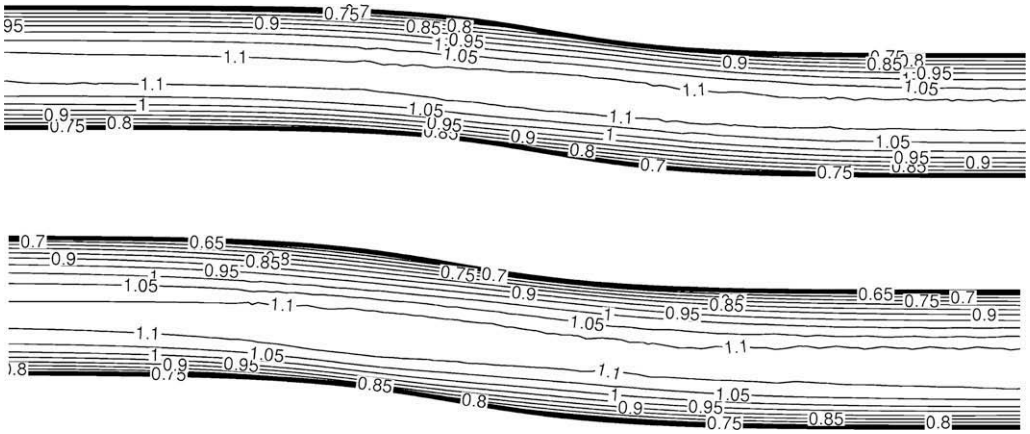

Fig. 9. Curved duct, starting shape. Primal (top) and adjoint (bottom) velocity magnitude ($|v|$ and $|u|$, respectively) contours.

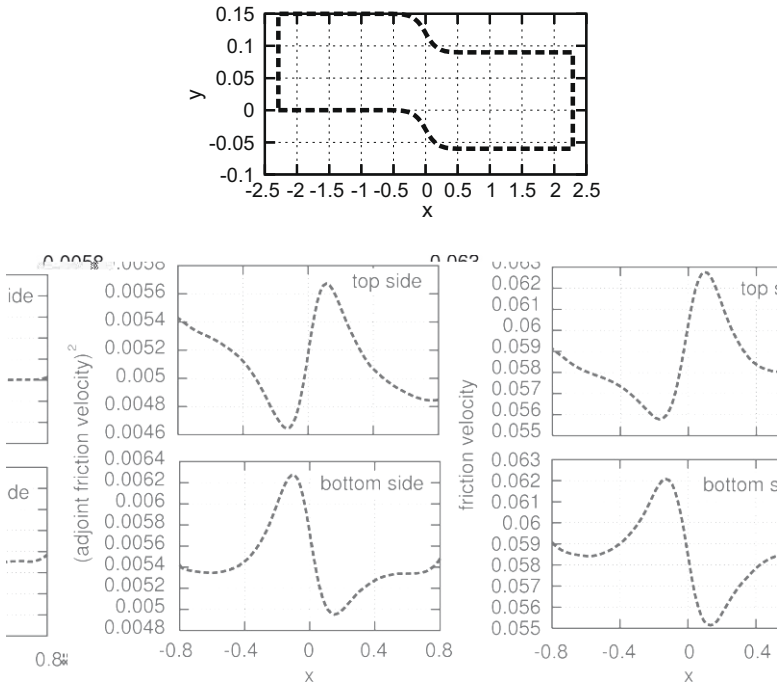

Fig. 10. Curved duct, starting shape, not in scale. (Left) Squared adjoint friction velocity u_τ^2 distributions along the upper and lower walls, in the vicinity of the bend. (Right) Primal friction velocity v_τ distribution.

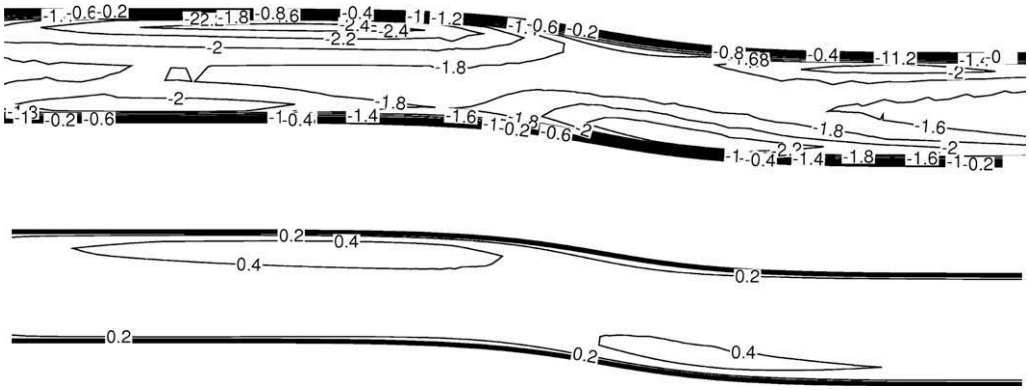

Fig. 11. Curved duct, starting shape. Adjoint k_a (top) and adjoint ε_a (bottom) contours.

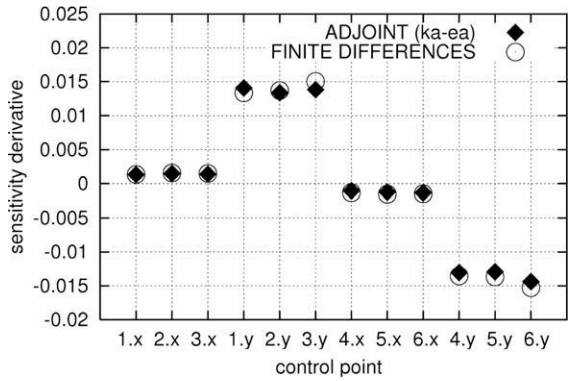

Fig. 12. Curved duct, starting shape. Sensitivity derivatives with respect to the design parameters. Control points 1–3 correspond to the lower wall, while 4–6 to the upper one.

In the second test case, the turbulent flow in a S-shaped duct is examined. The Reynolds number based on the inlet duct height is equal to $Re = 3 \times 10^4$. The parametrization of the duct is carried out using ten Bézier control points; half of them are used to model the upper and the other half the lower wall of the duct. Six out of the 10 control points (i.e. three on each side) are allowed to vary in both the x and y directions. An unstructured grid with 4215 nodes and 7848 triangular elements is used and the non-dimensional distance of the first nodes off the wall is, y^+, is close to 40 for all wall nodes. The primal and the adjoint velocity fields are shown in Fig. 9. The distribution of the squared adjoint friction velocity, u_τ^2, is shown in Fig. 10 (left) next to the primal friction velocity distribution (right). Using these figures, we may reconfirm the conclusions drawn in the first case. Along the curved walls, the proportionality between u_τ^2 and v_τ, as dictated by Eq. (38), can also be reconfirmed. The solution of the flow equations costs about 3 min on a 64 bit Quad Core Xeon processor whereas that of the adjoint equations costs as much as 3.5 min, using a point-implicit Jacobi solver. Finite differences have also been checked to be independent of the step size eps value used. This study is similar to that presented in the first case and is omitted herein.

Table 3
Curved duct: sensitivity derivative values computed using the proposed adjoint approach (AV), the adjoint approach with frozen turbulence (FT) and finite differences with $eps = 10^{-5}$ (FD).

	$\frac{\delta F}{\delta b_{1x}}10^{-2}$	$\frac{\delta F}{\delta b_{2x}}10^{-2}$	$\frac{\delta F}{\delta b_{3x}}10^{-2}$	$\frac{\delta F}{\delta b_{1y}}10^{-2}$	$\frac{\delta F}{\delta b_{2y}}10^{-2}$	$\frac{\delta F}{\delta b_{3y}}10^{-2}$
AV	0.132350	0.146288	0.138355	1.408965	1.338328	1.383206
FT	0.079660	0.092165	0.080026	0.646869	0.657732	0.680766
FD	0.134748	0.155444	0.149410	1.335599	1.371520	1.504939
	$\frac{\delta F}{\delta b_{4x}}10^{-2}$	$\frac{\delta F}{\delta b_{5x}}10^{-2}$	$\frac{\delta F}{\delta b_{6x}}10^{-2}$	$\frac{\delta F}{\delta b_{4y}}10^{-2}$	$\frac{\delta F}{\delta b_{5y}}10^{-2}$	$\frac{\delta F}{\delta b_{6y}}10^{-2}$
AV	−0.104727	−0.123075	−0.133411	−1.303809	−1.293449	−1.439183
FT	−0.035169	−0.049470	−0.065510	−0.499948	−0.594848	−0.746616
FD	−0.131045	−0.153260	−0.146802	−1.354187	−1.369399	−1.527819

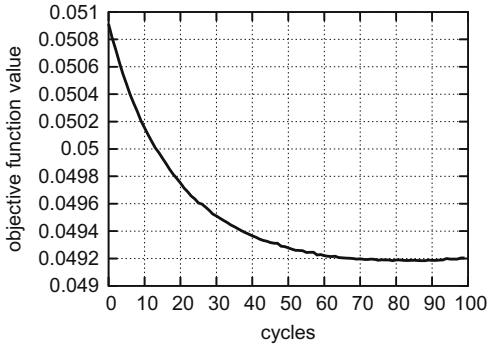

Fig. 13. Curved duct. Reduction of the objective function value (total pressure losses between the inlet and the outlet) in the course of the optimization.

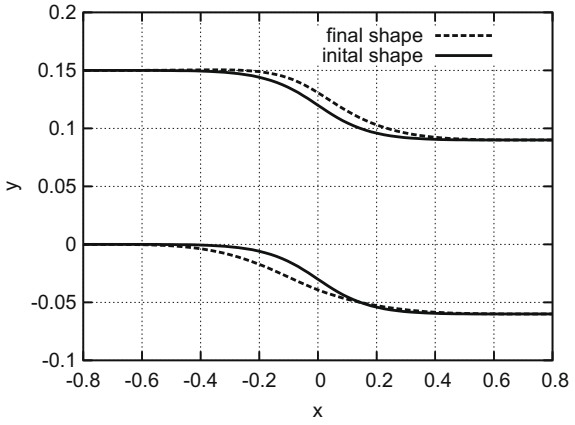

Fig. 14. Curved duct. Starting and final (optimal) duct shapes.

Moreover, in Fig. 11, the computed fields of the adjoint turbulence variables k_a and ε_a are presented. In Fig. 12 and Table 3, it is shown that the sensitivity derivatives of J, computed using the proposed adjoint approach and finite differences, are in excellent agreement and there are differences between them and the values computed by the incomplete adjoint approach. As in the first test case, an optimization was carried out, employing the computed sensitivity derivatives in a steepest descent algorithm. The convergence history of the objective function in each optimization cycle is shown in Fig. 13. The starting and final duct shapes, after the 100 steepest-descent cycles (based on exact derivatives but not necessarily the optimal descent step) are plotted in Fig. 14.

4. Conclusions – generalization of the method

The continuous adjoint method has been extended to cases in which the state equations are based on high Reynolds number turbulence models and the wall function technique. Through the introduction and use of the adjoint law of the wall, the adjoint system of pde's can be treated similarly to the state equations, by avoiding the differentiation of the adjoint variables close to the solid walls. The proposed adjoint formulation is exact, as demonstrated using the two examined test problems where the comparison of the so-computed sensitivity derivatives with finite differences is excellent. This paper provided a thorough study of the adjoint (mean flow and turbulence) inlet–outlet boundary conditions. Along the outlet, in particular, alternative ways to impose boundary conditions, with indistinguishable effects on the computed sensitivities, were described.

The proposed method can easily be extended to other functionals and/or eddy-viscosity type turbulence models other than the k–ε one, still based on the wall function technique. Also, this paper employed the wall function technique by assuming that the "real" solid wall lies at a user-defined distance underneath the grid boundary (marked as "solid wall", throughout this paper) where slip conditions (non-zero velocity driven by the friction velocity computed via the wall functions) are imposed. However, this is not restrictive at all; the reader may adjust the proposed formulation to the alternative wall function variant which employs no-slip conditions at the boundary nodes (which, thus, coincide with the real solid wall). In such a case, it is expected that different adjoint boundary conditions and a different definition of the adjoint friction velocity will be derived. From the discretization point of view, switching from vertex-centered to cell-centered finite volume schemes is also possible, despite the unavoidable changes to the way adjoint boundary conditions at the solid walls are employed. Finally, though we dealt with an objective function which comprises boundary integrals along the inlet and the outlet of the domain, the proposed method can be used with any other objective functions. For instance, in inverse design problems or drag minimization problems, where the objective function consists of integrals along the solid walls. This will introduces some extra terms (and eliminate some other) that can be taken into consideration with no extra difficulties.

Acknowledgments

This research work was funded by Volkswagen AG (Group Research, K-EFFG/V, Wolfsburg, Germany). The first author was supported by a grant from the State Scholarships Foundation, Greece.

References

[1] R. Martins, I.M. Kroo, J. Alonso, An automated method for sensitivity analysis using complex variables, AIAA Paper 2000-0689, 2000.
[2] J.C. Newman, W.K. Anderson, D.L. Whitfield, Multidisciplinary sensitivity derivatives using complex variables, Tech. Rep. MSSU-COE-ERC-98-08.
[3] S. Hazra, V. Schulz, J. Brezillon, N. Gauger, Aerodynamic shape optimization using simultaneous pseudo-timestepping, Journal of Computational Physics 204 (1) (2005) 46–64.
[4] O. Pironneau, On optimum design in fluid mechanics, Journal of Fluid Mechanics 64 (1974) 97–110.
[5] A. Jameson, Aerodynamic design via control theory, Journal of Scientific Computing 3 (1988) 233–260.
[6] W.K. Anderson, V. Venkatakrishnan, Aerodynamic design optimization on unstructured grids with a continuous adjoint formulation, AIAA Paper 97-0643, 1997.
[7] D.I. Papadimitriou, K.C. Giannakoglou, A continuous adjoint method with objective function derivatives based on boundary integrals for inviscid and viscous flows, Computers and Fluids 36 (2007) 325–341.
[8] G.R. Shubin, P.D. Frank, A comparison of the implicit gradient approach and the variational approach to aerodynamic design optimization, Boeing Computer Services Report AMS-TR-163, 1991.
[9] G.W. Burgreen, O. Baysal, Three-dimensional aerodynamic shape optimization using discrete sensitivity analysis, AIAA Journal 34 (9) (1996) 1761–1770.
[10] J. Elliot, J. Peraire, Aerodynamic design using unstructured meshes, AIAA Paper 96-1941, 1996.
[11] M.C. Duta, M.B. Giles, M.S. Campobasso, The harmonic adjoint approach to unsteady turbomachinery design, International Journal for Numerical Methods in Fluids 40 (3–4) (2002) 323–332.
[12] C. Othmer, A continuous adjoint formulation for the computation of topological and surface sensitivities of ducted flows, International Journal for Numerical Methods in Fluids 58 (8) (2008) 861–877.
[13] A. Jameson, N. Pierce, L. Martinelli, Optimum aerodynamic design using the Navier–Stokes equations, Theoretical and Computational Fluid Dynamics 10 (1998) 213–237.
[14] A.S. Zymaris, D.I. Papadimitriou, K.C. Giannakoglou, C. Othmer, Continuous adjoint approach to the Spalart–Allmaras turbulence model for incompressible flows, Computers and Fluids (2008), doi:10.1016/j.compfluid.2008.12.006.
[15] P. Spalart, S. Allmaras, A one-equation turbulence model for aerodynamic flows, AIAA Paper 92-0439, 1992.
[16] E.J. Nielsen, J. Lu, M.A. Park, D.L. Darmofal, An implicit exact dual adjoint solution method for turbulent flows on unstructured grids, Computers and Fluids 33 (2004) 1131–1155.
[17] D.W. Zingg, T.M. Leung, L. Diosady, A.H. Truong, S. Elias, M. Nemec, Improvements to a Newton–Krylov adjoint algorithm for aerodynamic optimization, AIAA Paper 2005-4857, 2005.

[18] R.P. Dwight, J. Brezillon, Effect of approximations of the discrete adjoint on gradient-based optimization, AIAA Journal 44 (12) (2006) 3022–3031.
[19] W.K. Anderson, D.L. Bonhaus, Airfoil design on unstructured grids for turbulent flows, AIAA Journal 37 (2) (1999) 185–191.
[20] B.J. Lee, C. Kim, Automated design methodology of turbulent internal flow using discrete adjoint formulation, Aerospace Science and Technology 11 (2007) 163–173.
[21] D.J. Mavriplis, Discrete adjoint-based approach for optimization problems on three-dimensional unstructured meshes, AIAA Journal 45 (4) (2007) 740–750.
[22] C.S. Kim, C. Kim, O.H. Rho, Feasibility study of constant eddy-viscosity assumption in gradient-based design optimization, Journal of Aircraft 40 (6) (2003) 1168–1176.
[23] C.H. Norris, W.C. Reynolds, Turbulent channel flow with a moving wall boundary, Rept. No. FM-10, Stanford University, Rept. Mech. Eng., 1975.
[24] W. Rodi, G. Scheuerer, Scrutinizing the k–ε model under adverse pressure gradient conditions, Journal of Fluids Engineering 108 (1986) 174–179.
[25] W. Rodi, Experience with two-layer models combining the k–ε model with a one-equation model near the wall, AIAA Paper 91-0216, 1991.
[26] D.L. Sondak, R.H. Pletcher, Application of wall function to generalized nonorthogonal curvilinear coordinate systems, AIAA Paper 93-3107, 1993.
[27] W. Cabot, P. Moin, Approximate wall boundary conditions in the large-eddy simulation of high Reynolds number flow, Flow Turbulence and Combustion 63 (1999) 269–291.
[28] J.A. Templeton, M. Wang, P. Moin, Towards LES wall models using optimization techniques, Center for Turbulent Research, Annual Research Briefs, 2002.
[29] C. Pantano, D.I. Pullin, P.E. Dimotakis, G. Matheou, LES approach for high Reynolds number wall-bounded flows with application to turbulent channel flow, Journal of Computational Physics 227 (2008) 9271–9291.
[30] E.Y.K. Ng, H.Y. Tan, H.N. Lim, D. Choi, Near-wall function for turbulence closure models, Computational Mechanics 29 (2002) 178–181.
[31] D.I. Papadimitriou, K.C. Giannakoglou, Aerodynamic shape optimization using adjoint and direct approaches, Archives of Computational Methods in Engineering 15 (4) (2008) 447–488.
[32] S. Nadarajah, A. Jameson, Optimal control of unsteady flows using a time accurate method, AIAA Paper 2002-5436, 2002.
[33] S. Nadarajah, M. McMullen, A. Jameson, Non-linear frequency domain based optimum shape design for unsteady three-dimensional flow, AIAA Paper 2002-2838, 2002.
[34] A.L. Marsden, M. Wang, J.E. Dennis, P. Moin, Suppression of vortex shedding noise via derivative-free shape optimization, Stanford University.
[35] W. Jones, B. Launder, The prediction of laminarization with a two-equation model of turbulence, Int. J. Heat Mass Transfer 15 (1972) 301–314.
[36] A.J. Chorin, A numerical method for solving incompressible viscous flow problems, Journal of Computational Physics 2 (1967) 12–26.
[37] P. Roe, Approximate Riemann solvers, parameter vectors, and difference schemes, Journal of Computational Physics 43 (1981) 357–371.